IEEE Access
Multidisciplinary | Rapid Review | Open Access Journal

Received September 7, 2018, accepted October 14, 2018, date of publication November 15, 2018, date of current version February 4, 2019.

Digital Object Identifier 10.1109/ACCESS.2018.2881440

Design and Application of MVIC for Hydraulic Drive Unit of Legged Robot

BIN YU[1,2], (Member, IEEE), KAIXIAN BA[1], (Member, IEEE), YALIANG LIU[1], ZHENGGUO JIN[1], QIXIN ZHU[1], ZHENGJIE GAO[1], (Student Member, IEEE), GUOLIANG MA[1], (Student Member, IEEE), AND XIANGDONG KONG[1,2]

[1]School of Mechanical Engineering, Yanshan University, Qinhuangdao 066004, China
[2]School of Mechanical Engineering, Nanjing Institute of Technology, Nanjing 211167, China

Corresponding author: Qixin Zhu (qixinz@ysu.edu.cn)

This work was supported in part by the China Postdoctoral Science Foundation under Grant 2018M640246, in part by the National Natural Science Foundation of China under Grant 51605417, and in part by Hebei Military and Civilian Industry Development Funds Projects 2018B030.

ABSTRACT A hydraulic drive unit (HDU), applied in each joint of a hydraulic driven legged robot, usually adopts the impedance control outer loop based on the hydraulic position or the force control inner loop during the motion process. When the hydraulic control adopts closed-loop force control, its control performance can directly determine the control performance of the impedance control outer loop. Therefore, it is significant to design a high-accuracy force control method aimed at HDUs. In this paper, aiming at the above research concept, the force control system of the HDU is introduced first, and the lack of the force control performance is studied under different working conditions on the HDU performance test platform. Second, a model-based variable input controller (MVIC) is designed to improve the force control performance. Finally, the control performance of the MVIC is verified on the HDU performance test platform. The experimental results show that the MVIC can greatly improve the force control accuracy under different working conditions and that the controller has good robustness. The above research results can provide important reference and lay the experimental foundation for force-based impedance control.

INDEX TERMS Legged robot, hydraulic drive unit (HDU), force control, model-based variable input control (MVIC).

I. INTRODUCTION

Legged robots are better at adapting to unknown and unstructured environments than wheeled robots [1], crawler robots [2], and spherical robots [3]. Their unique advantages, such us overcoming obstacles and executing tasks in the wild, have made them a major focus of research in the field of robotics. For robotic drive mode, motor drive, pneumatic drive, and hydraulic drive are generally employed. However, legged robots with hydraulic drive are superior to those that adopt other drive modes. Hydraulic drive mode enables such robots to have greater power-to-weight ratios, higher load capacities, faster response speeds, and other excellent characteristics. Nowadays, highly integrated valve-controlled cylinders, called hydraulic drive units (HDUs), are utilized to drive the joints of hydraulic drive legged robots [4]–[6]. However, various robot control issues still exist. For example, during the walking process of legged robots, especially on different types of ground such as grass, dessert, and snow, different obstacles are encountered, making it more difficult to control such robots because the load characteristics of the ends of their feet change with the environment. Furthermore, although the adoption of HDUs has resulted in high-performance robot control, their hydraulic systems still exhibit problems, such as strong nonlinearity, and time-varying parameters. Consequently, robot control is very difficult and complex.

The impedance control is a common control method for the legged robot during the actual motion process. It aims to make the leg joint of the robot compliant, making the whole leg of the robot equivalent to a second-order mass-spring-damping system with the desired stiffness, damping, and mass. This control method has been successfully applied to different motor-driven legged robots, such as Tekken [7], Scout [8], kinetically ordered locomotion test(KOLT) [9], MIT Cheetah robot [10] and humanoid Roboray [11] In recent years, as the hydraulic driven legged robot gradually has become a popular research trend, the impedance control method has also been applied to this kind of robot, such as BigDog [12],

Hydraulic Quadruped(HyQ) [13], Scalf-1 [14], Light-Weight Robot(LWR) [15], StarlETH [16], Legged Squad Support System(LS3) [17], JINPOONG [18], and Atlas [19] In the application of the hydraulic drive legged robot described above, When the hydraulic system control method is the closed-loop force control, the impedance control method is called force-based impedance control. The force control accuracy should be high enough so that the control inner loop accuracy does not affect the impedance control outer loop accuracy. However, for the complex and variable load environment and the natural problem of the hydraulic system, the force control accuracy cannot reach the requirements under actual conditions. Therefore, it is necessary to improve the control accuracy of the force control inner loop to enhance the overall impedance control accuracy and the overall motion performance of the legged robot.

In recent years, many scholars from many countries have carried out a large amount of research on the high accuracy and robustness of the force control system, but this research has focused not only on the hydraulic force control system but also methods such as backstepping control [20], fuzzy intelligent control [21], [22], quantitative feedback theory [23], [24] and robust control [25], [26]. The references described above use many advanced control methods to improve the control performance (such as tracing accuracy, response speed and disturbance rejection ability), and it has a very good control effect, but most of these advanced control algorithms are not based on the mathematical model of the system in the control operation and have certain complexity in engineering applications. The most important factor is that these advanced force control algorithms are not independently designed for impedance control and do not consider the diversity of the input signal during the actual motion process of the robot and the complexity of the load environment. When an HDU adopts force-based impedance control, its force control inner loop is actually a double-input and single-output system; to make the system achieve high control performance, the improvement should address two aspects: first, the system should have a good disturbance rejection ability when the force output is affected by the external disturbance position so that the force output is not affected by the disturbance as much as possible. Second, the system should have excellent force tracing performance when the force input produced by the impedance control outer loop is input into the system.

In previous research by the author, force control performance and its parameter sensitivity of the HDU were studied in many aspects, providing an accurate force control mathematical model for this paper [5], [27]. Moreover, the dynamic compliance of the position control system and the force control system of the HDU were researched, and a compliance-reduced controller and compliance-enhanced controller were designed to improve the disturbance rejection ability of both the position and force control system [28], [29]. However, the above research results only improved the disturbance rejection ability when the system has no input. The above controller cannot improve the tracing capability of the system during the actual motion process because of the complex and variable inner loop input signal, thus limiting the application of the above controller.

The main contribution of this paper is a model-based variable input controller (MVIC) designed by mechanism modeling, which aims to improve the two aspects that affect the force control performance of the HDU discussed above. Based on the above idea, the organization of the whole paper is as follows: the mathematical model of the HDU force control system is introduced first, and then the force control performance of the system is tested under different working conditions on the HDU performance test platform. Second, due to the lack of the HDU force control performance in the test, a novel control compensation strategy is discussed, and based on this strategy, the MVIC containing the natural nonlinearity and load characteristics of the hydraulic system is designed. Finally, the experiment is conducted by using the MVIC through the HDU performance test platform. With different input signals, the force tracing error is analyzed quantitatively.

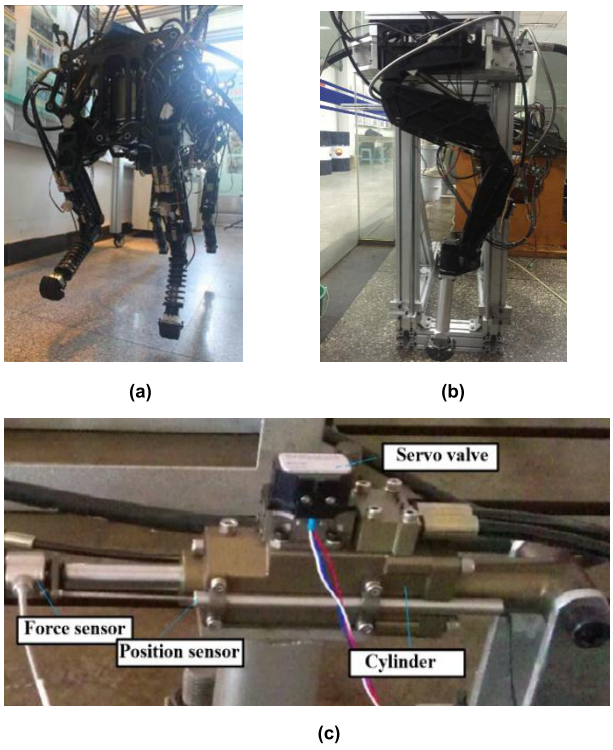

FIGURE 1. Photos of test platform. (a) Prototype of quadruped robot. (b) Leg hydraulic drive system. (c) HDU.

II. INTRODUCTION OF HDU FORCE CONTROL SYSTEM

The HDU is a highly integrated system of servo valve-controlled symmetrical cylinders. The prototype of a quadruped robot, leg hydraulic drive system test platform and HDU test platform are shown in (a), (b) and (c) in Fig. 1.

The closed-loop force control transfer block diagram of the HDU is shown in Fig. 2 The derivation in detail and performance analysis are presented in previous research by the author [27], [29].

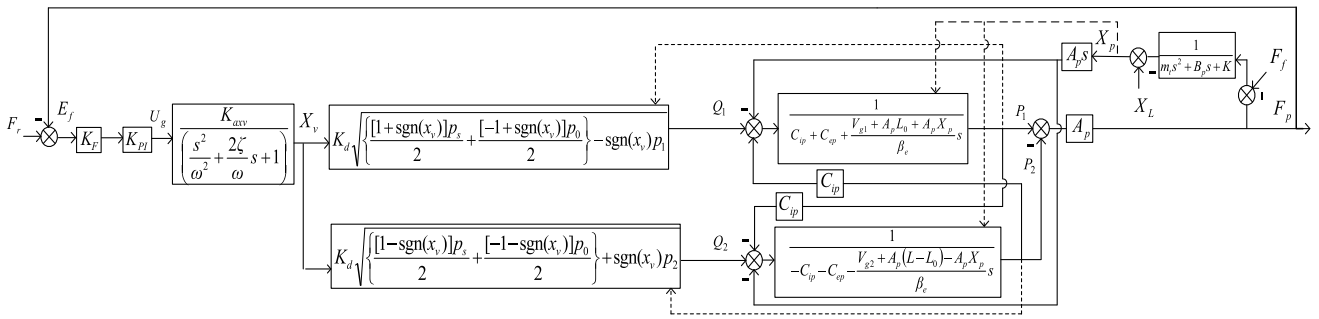

FIGURE 2. Closed-loop force control transfer block diagram of the HDU.

In Fig. 2, ω is the natural frequency of the servo valve, ζ is the damping ratio of the servo valve, $K_d = C_d W\sqrt{2/\rho}$ (K_d is defined as the conversion coefficient in this paper), C_d is the orifice flow coefficient of the spool valve, W is the area gradient of the spool valve, ρ is the density of the hydraulic oil, p_s is the system supply oil pressure, p_1 is the left cavity pressure of the servo cylinder, p_2 is the right cavity pressure of the servo cylinder, p_0 is the system return oil pressure, C_{ip} is the internal leakage coefficient of the servo cylinder, C_{ep} is the external leakage coefficient of the servo cylinder, A_p is the effective piston area of the servo cylinder, β_e is the effective bulk modulus, m_t is the conversion mass (including the piston, the displacement sensor, the force sensor, the connecting pipe and the oil in the servo cylinder), F_r is the input force, K_F is the force sensor gain, K_{PI} is the PI controller gain including the proportional gain K_P and the integral gain K_I, K_{axv} is the servo valve gain, K is the load stiffness, B_p is the load damping, X_L is the load position, X_v is the servo valve spool displacement, X_p is the servo cylinder piston displacement, V_{g1} is the volume of the input oil pipe, V_{g2} is the volume of the output oil pipe, F_f is the friction, U_g is the controller output voltage, Q_1 is the inlet oil flow, and Q_2 is the outlet oil flow.

The force control error E_f in Fig. 2 consists of two parts, which are expressed as follows.

$$E_f = F_r - F_p \tag{1}$$

In Eq. (1), E_{f1} represents the force error generated by the influence of the disturbance position on the position control. E_{f2} represents the trace error between the input and output of the inner loop control. Both of these two aspects determine the force control performance. Therefore, the theoretical analysis and experiment in the following paper will be used to further study E_{f1} and E_{f2}.

III. MVIC

A. DESIGN STRATEGY FOR CONTROLLER

The force control system has two input variables, F_r and X_L the former variable is controllable, and the latter one is uncontrollable. Thus, a new control idea emerges. The only controllable variable F_r can be changed into F_r' through a controller called the MVIC. After F_r' enters the system, the corresponding output F_p' could approach F_r more precisely. Based on the above ideas, this section proposes the control strategy shown in Fig. 3.

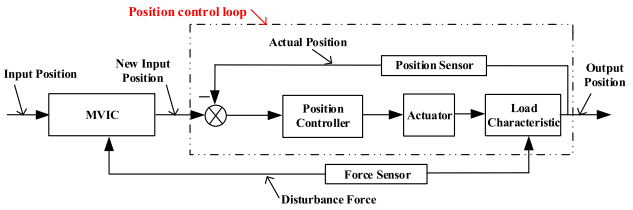

FIGURE 3. Control strategy of the MVIC.

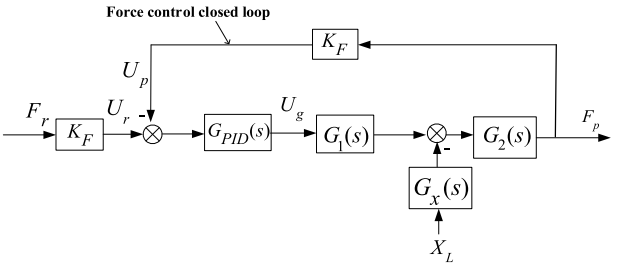

FIGURE 4. The HDU force control transfer block diagram.

B. CONTROLLER DESIGN

Based on Fig. 2, the HDU force control transfer block diagram can be expressed as shown in Fig. 4.

In Fig. 4, $G_x(s)$ is the transfer function applied to the system by the disturbance position. $G_1(s)$, $G_2(s)$ is the transfer function of the system. These three transfer functions are shown as follows. Due to the limited space, the detail derivation of the above three transfer functions is not shown in this paper.

$$G_1(s) = \frac{k_1V_2 + k_2V_1}{\beta_e} A_p \left(m_t s^2 + B_p s + K\right) \frac{K_{axv}}{\frac{s^2}{\omega^2} + \frac{2\zeta}{\omega}s + 1} \tag{2}$$

$$G_2(s) = \frac{1}{\frac{m_tV_1V_2}{\beta_e^2}s^3 + \frac{\beta_e m_t C_{ip}(V_1+V_2) + B_pV_1V_2}{\beta_e^2}s^2 + \left[\frac{KV_1V_2}{\beta_e^2} + \frac{(B_pC_{ip} + A_p^2)(V_1+V_2)}{\beta_e}\right]s + \frac{KC_{ip}(V_1+V_2)}{\beta_e}} \tag{3}$$

$$G_x(s) = \frac{V_1 + V_2}{\beta_e} A_p^2 s(m_t s^2 + B_p s + K) \tag{4}$$

In Fig. 4, the transfer function of the HDU force control system can be expressed as follows:

$$\Phi_f(s) = \frac{F_p}{F_r} = \frac{K_F G_{PID} G_1(s) G_2(s) - \frac{X_L}{F_r} G_x(s) G_2(s)}{1 + K_F G_{PID} G_1(s) G_2(s)}. \tag{5}$$

At this point, the error transfer function of the HDU force control system can be expressed as follows:

$$\begin{aligned}\Phi_{fe}(s) &= 1 - \Phi_f(s) \\ &= 1 - \frac{K_F G_{PID} G_1(s) G_2(s) - \frac{X_L}{F_r} G_x(s) G_2(s)}{1 + K_F G_{PID} G_1(s) G_2(s)} \\ &= \frac{1 + \frac{X_L}{F_r} G_x(s) G_2(s)}{1 + K_F G_{PID} G_1(s) G_2(s)}.\end{aligned} \tag{6}$$

Obviously, the error of the system is related to the disturbance position X_L, and the numerator of Eq. (6) is

$$1 + \frac{X_L}{F_r} G_x(s) G_2(s) \neq 0. \tag{7}$$

Eq. (7) shows that the error transfer function of the system is not zero.

Combined with the control strategy in Section III.A, Eq. (7) can be transformed into:

$$\Phi_f'(s) = \frac{F_p}{F_r'} \cdot \frac{F_r'}{F_r}. \tag{8}$$

In Eq. (8), $F_p/F_r{}'$ represents the transfer function of the HDU force control system when the input force is F_r'. The combination of Eq. (5), and Eq. (8) can be expressed as follows:

$$\begin{aligned}\Phi_f'(s) &= \frac{Fp}{F_r} = \frac{F_p}{F_r'} \cdot \frac{F_r'}{F_r} \\ &= \frac{K_F G_{PID} G_1(s) G_2(s) - \frac{X_L}{F_r'} G_x(s) G_2(s)}{1 + K_F G_{PID} G_1(s) G_2(s)} \cdot \frac{F_r'}{F_r}.\end{aligned} \tag{9}$$

At this point, the error transfer function can be expressed as follows:

$$\begin{aligned}\Phi_{fe}(s) &= 1 - \Phi_f'(s) \\ &= \frac{F_r\left[1 + K_F G_{PID} G_1(s) G_2(s)\right] - \left[F_r' K_F G_{PID} G_1(s) G_2(s) - X_L G_x(s) G_2(s)\right]}{F_r\left[1 + K_F G_{PID} G_1(s) G_2(s)\right]}.\end{aligned} \tag{10}$$

To make the systematic error zero, the numerator in Eq. (10) needs to be zero, and then the numerator of Eq. (10) can be expressed as:

$$\begin{aligned}&F_r\left[1 + K_F G_{PID} G_1(s) G_2(s)\right] \\ &\quad - \left[F_r' K_F G_{PID} G_1(s) G_2(s) - X_L G_x(s) G_2(s)\right] = 0.\end{aligned} \tag{11}$$

Eq. (11) can be transformed as:

$$F_r' = \left(1 + \frac{1}{K_F G_{PID} G_1(s) G_2(s)}\right) \cdot F_r + \frac{G_x(s)}{K_F G_{PID} G_1(s)} \cdot X_L. \tag{12}$$

When the new input force of the system is F_r', the new output force generated by the system will approach the desired input force F_r. This can theoretically improve the accuracy of the force control, and the system should have high robustness under different disturbance positions.

The block diagram of the force control system after adopting the MVIC is shown in Fig. 5.

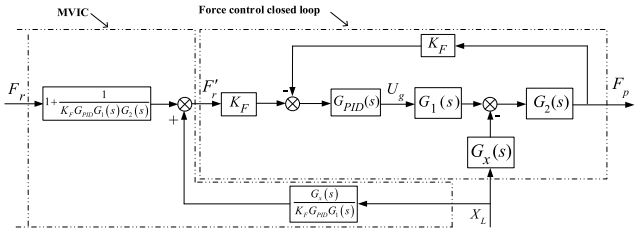

FIGURE 5. Block diagram of the force control system after adopting the MVIC.

The effects of the initial position of the HDU are ignored to simplify the control compensation link, so:

$$V_1 = V_2 = V_t/2. \tag{13}$$

Inserting Eq. (2), (3), (4) and (13) into Eq. (12), then Eq. (12) can be expressed as (14), shown at the bottom of this page.

Eq. (14) is the complete expression of the MVIC. The disturbance position signal tested by the position sensor is an analog voltage signal whose value has high frequency noise. The compensation voltage generated from Eq. (14), which still contains second order and even higher order links. fluctuates observably, decreasing the control effect dramatically. Therefore, part of Eq. (14) needs to be optimized with respect to the second order and above. Therefore, Eq. (14) can be simplified as follows:

$$\begin{aligned}F_r' = &\left\{\begin{array}{l}\frac{4\beta_e m_t C_{ip} + B_p V_t}{2\beta_e} + \frac{2\zeta}{\omega}\left[\frac{KV_t}{2\beta_e} + 2(B_p C_{ip} + A_p^2)\right] \\ + \frac{2KC_{ip}}{\omega^2} + K_F K_{PI} K_{axv} A_p m_t (k_1 + k_2)\end{array}\right\} s^2 \\ &+ \left[\begin{array}{l}\frac{4\zeta K C_{ip}}{\omega} + \frac{KV_t}{2\beta_e} + 2(B_p C_{ip} + A_p^2) \\ + K_F K_{PI} K_{axv} A_p (k_1 + k_2) B_p\end{array}\right] s \\ &+ K\left[2C_{ip} + K_F K_{PI} K_{axv} A_p (k_1 + k_2)\right] \\ &\overline{K_F K_{PI} K_{axv} A_p (k_1 + k_2)\left(m_t s^2 + B_p s + K\right)} \\ &\cdot F_r + \frac{4A_p \zeta s^2/\omega + 2A_p s}{K_F K_{PI} K_{axv}(k_1 + k_2)} \cdot X_L\end{aligned} \tag{15}$$

$$F_r' = \left\{1 + \frac{\left(\frac{s^2}{\omega^2} + \frac{2\zeta}{\omega} s + 1\right)\left[\left(m_t s^2 + B_p s + K\right)\left(\frac{V_t s}{2\beta_e} + 2C_{ip}\right) + 2A_p^2 s\right]}{K_F K_{PI} K_{axv} A_p (k_1 + k_2)\left(m_t s^2 + B_p s + K\right)}\right\} \cdot F_r + \frac{2A_p s\left(\frac{s^2}{\omega^2} + \frac{2\zeta}{\omega} s + 1\right)}{K_F K_{PI} K_{axv}(k_1 + k_2)} \cdot X_L. \tag{14}$$

where k_1+k_2 is the nonlinearity link, which can be expressed as follows:

$$k_1 + k_2 = 2\sqrt{P_s - P_0 - \hat{P}_L}. \tag{16}$$

Inserting Eq. (15) into Eq. (14), the result is as follows:

$$F_r' = \frac{\begin{bmatrix} m_t C_{ip} + \frac{B_p V_t}{4\beta_e} + \frac{2\zeta}{\omega}\left(\frac{KV_t}{4\beta_e} + A_p^2\right) \\ +B_p C_{ip} \\ +\frac{KC_{ip}}{\omega^2} + K_F K_{PI} K_{axv} A_p m_t \sqrt{p_s - p_0 - \hat{p}_L} \end{bmatrix} s^2}{K_F K_{PI} K_{axv} K_d A_P \left(m_t s^2 + B_p s + K\right)\sqrt{p_s - p_0 - \hat{p}_L}}$$
$$+ \frac{\begin{pmatrix} \frac{2\zeta K C_{ip}}{\omega} + \frac{KV_t}{4\beta_e} \\ +A_p^2 + B_p C_{ip} \\ +K_F K_{PI} K_{axv} A_p B_P \sqrt{p_s - p_0 - \hat{p}_L} \end{pmatrix} s + K\left[C_{ip} + K_F K_{PI} K_{axv} K_d A_P \sqrt{p_s - p_0 - \hat{p}_L}\right]}{K_F K_{PI} K_{axv} K_d A_P \left(m_t s^2 + B_p s + K\right)\sqrt{p_s - p_0 - \hat{p}_L}}$$
$$\cdot F_r + , \frac{2A_p \zeta s^2/\omega + A_p s}{K_F K_{PI} K_{axv} K_d \sqrt{p_s - p_0 - \hat{p_L}}} \cdot X_L. \tag{17}$$

Eq. (16) is the simplified expression of the MVIC.

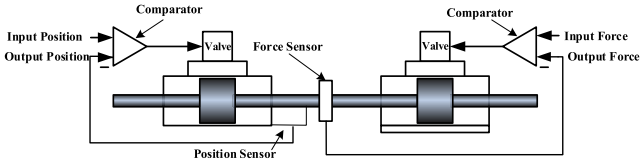

FIGURE 6. Schematic of HDU performance test platform.

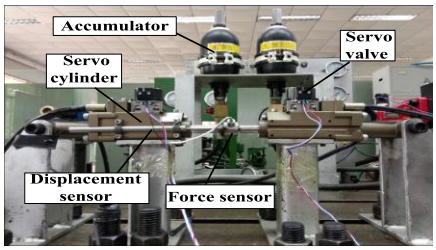

FIGURE 7. Photos of HDU performance test platform.

IV. EXPERIMENT OF MVIC PERFORMANCE

A. INTRODUCTION OF HDU PERFORMANCE TEST PLATFORM

The schematic of the HDU performance test platform is shown in Fig. 6. The photo of the HDU performance test platform is shown in Fig. 7. Through the HDU performance test platform, the control performance of the HDU position control system is tested. The left part contains a servo valve-controlled cylinder and a position sensor which adopts position closed loop control. The right part contains a same servo valve-controlled cylinder and a force sensor which adopts force closed loop control. The detailed hydraulic schematic of the HDU test platform, hydraulic system composition and electric system composition, can be found in the author's previous research [27], [28]. Due to limited space, that research won't be listed in this paper.

B. EXPERIMENTAL PLAN

The sinusoidal signal is usually selected as the performance test signal. The trace characteristic of the system responding to the sinusoidal signal can be used to evaluate system performance. At the same time, the disturbance rejection performance can be tested under different sinusoidal disturbance positions. In addition, the force control performance of the HDU under a random force input signal and its corresponding disturbance position are also tested. The experimental plan is shown in Table 1.

TABLE 1. Experimental plan.

Working condition	Sinusoidal input force		Sinusoidal disturbance position		Random force signal
①	2000N	0.5 Hz	0 mm		
②	1000N	1 Hz	0 mm		⑨ Random force signal 1
③	0N		2 mm	1 Hz	
④	0N		4 mm	0.5 Hz	
⑤	1000N	1 Hz	2mm	0.5 Hz	
⑥	1000N	1 Hz	2mm	1 Hz	⑩ Random force signal 2
⑦	1000N	1 Hz	4mm	0.5 Hz	
⑧	1000N	1 Hz	4mm	1 Hz	

As shown in Table 1, the working conditions are divided into four parts:

First, working conditions ① and ② aim to test the force tracing performance under different amplitude and frequency inputs without a disturbance position

Second, working conditions ③ and ④ aim to test the disturbance rejection performance under different amplitudes and frequencies of the disturbance position without force input.

Third, working conditions ⑤ to ⑧ aim to test the force control performance under both force input and disturbance position.

Fourth, working conditions ⑨ to ⑩ aim to test the force control performance under a random force input and disturbance position.

C. EXPERIMENTAL RESULTS

To verify the validity of the MVIC designed in Section III, the integral separation PI controller designed in the author's previous research [27], [29] is used as a comparison reference. Under each working condition shown in Table 1. Four curves are presented to compare, the desired input force F_r, the new input force F_r', the output force F_p with MIVC and the output force F_p without MIVC. In addition, the controller is tested under more working conditions, and it also showed a satisfactory control effect. Due to limited space, the curves will not be shown in this paper. As shown in Table 1, the control effect curves are shown in Fig. 8 to Fig. 17.

The control effect under different working conditions from Fig.8 to Fig.17 can be quantitatively presented. The main performance indexes under different working conditions are listed in Table. 2. In Table. 2, the relative force error date

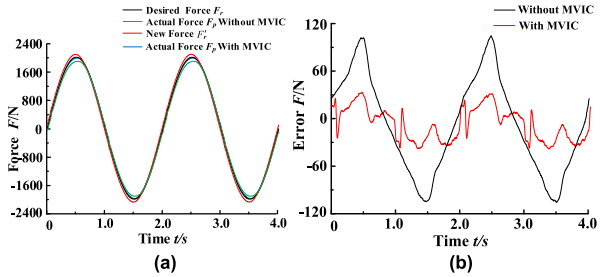

FIGURE 8. Experimental results of working condition ①. (a) Response curve. (b) Force error curve.

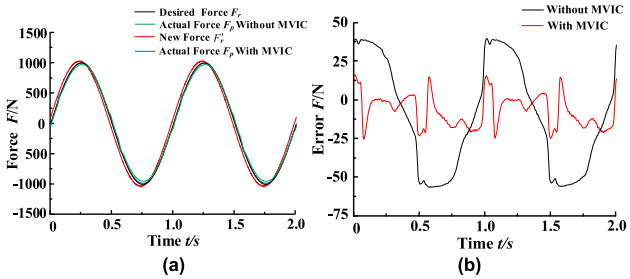

FIGURE 9. Experimental results of working condition ②. (a) Response curve. (b) Force error curve.

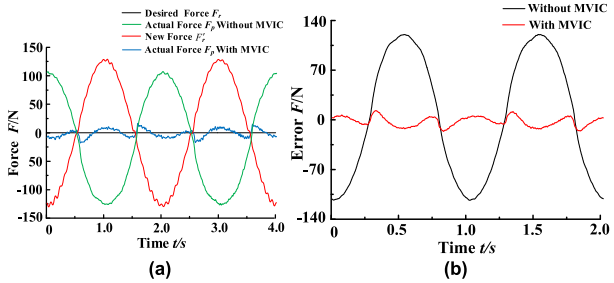

FIGURE 10. Experimental results of working condition ③. (a) Response curve. (b) Force error curve.

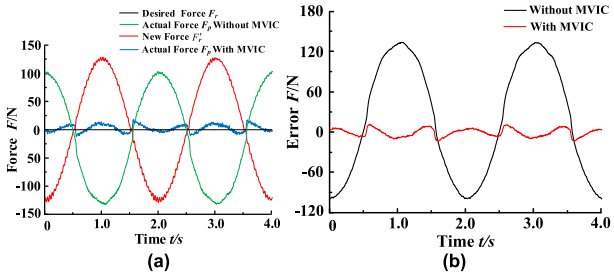

FIGURE 11. Experimental results of working condition ④. (a) Response curve. (b) Force error curve.

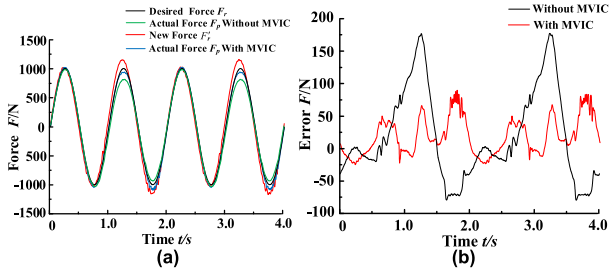

FIGURE 12. Experimental results of working condition ⑤. (a) Response curve. (b) Force error curve.

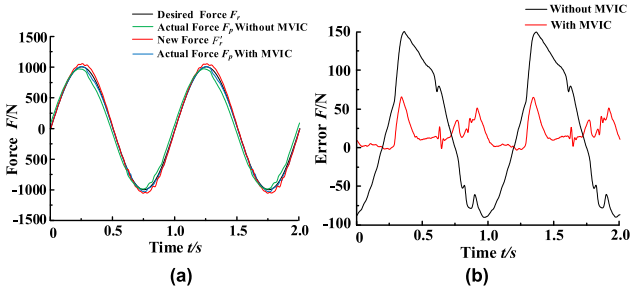

FIGURE 13. Experimental results of working condition ⑥. (a) Response curve. (b) Force error curve.

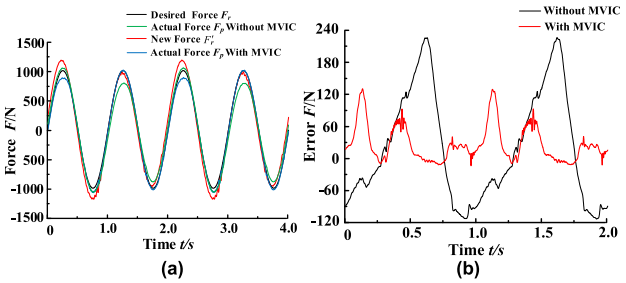

FIGURE 14. Experimental results of working condition ⑦. (a) Response curve. (b) Force error curve.

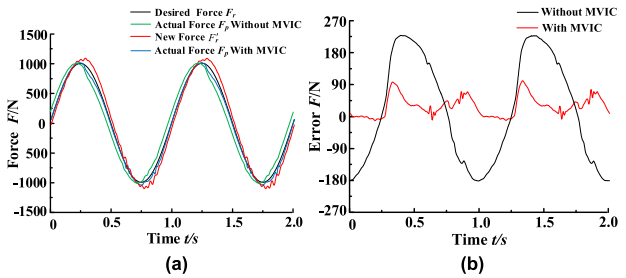

FIGURE 15. Experimental results of working condition ⑧. (a) Response curve. (b) Force error curve.

is expressed as absolute value. (Force error=desired force – actual force, Force error elimination ratio=(force error without MVIC – force error with MIVC)/ force error without MVIC).

According to Fig. 8 to Fig. 17 and Table. 2, it can be seen the following results:

1) THE RESULTS WITHOUT MVIC

Under working condition ① and ②, the HDU has good force control performance, the force error curves show that the force error also sinusoidally change with the sinusoidal input change. The peak force error is nearly 5% compared with the amplitude of input force. Under working condition ③ and ④, the disturbance rejection performance of the HDU force control system is not good, especially when the disturbance position has different amplitude and frequency. The force error curve has oppositely sinusoidal change with the sinusoidal disturbance position change. Under working condition ⑤ to ⑧, for the influence of the disturbance position on the

TABLE 2. Main performance indexes under different working conditions.

Working conditions \ Performance indexes		Peak value of force error (N)		Peak error elimination ratio (%)	Mean value of force error (N)		Mean error elimination ratio (%)
		Without MIVC	With MIVC		Without MIVC	With MIVC	
Sinusoidal input force	①	104.38	39.08	62.56	52.57	18.91	64.03
	②	55.56	25.71	53.73	28.49	10.28	63.90
	③	103.68	20.17	80.54	79.46	14.75	81.43
	④	132.15	28.01	78.80	79.83	15.64	80.40
	⑤	179.37	90.11	49.76	54.37	26.52	51.22
	⑥	146.90	62.41	57.51	72.90	16.20	77.78
	⑦	224.39	131.42	41.43	88.25	30.00	66.00
	⑧	227.89	100.34	55.97	135.10	30.65	77.31
Random force signal	⑨	1051.63	391.33	62.79	287.50	118.65	58.73
	⑩	1204.65	370.69	69.22	468.76	105.51	77.49

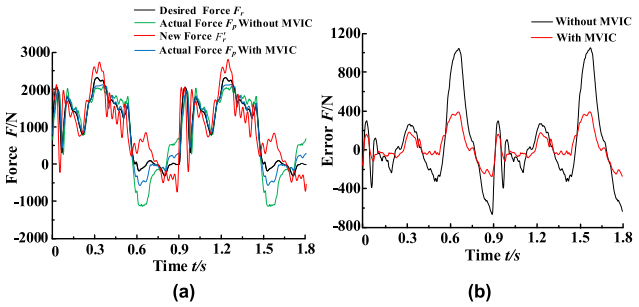

FIGURE 16. Experimental results of working condition ⑨. (a) Response curve. (b) Force error curve.

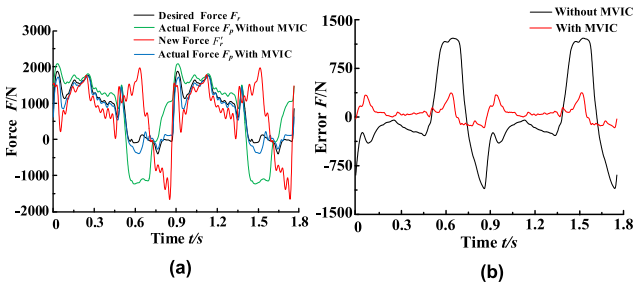

FIGURE 17. Experimental results of working condition ⑩. (a) Response curve. (b) Force error curve.

control performance is larger than that of input force, so the actual force appears phase angle advance phenomenon relative to the desired force. Under working condition ⑨ and ⑩, the robustness of the force control is poor under random force input and disturbance position.

2) THE RESULTS WITH MVIC

Under working condition ① and ②, the force control tracing performance is greatly improved, and the amplitude of the force error does not change obviously, and its sinusoidal variation is eliminated. For example, when the sinusoidal disturbance force has a frequency of 0.5 Hz, an amplitude of 2000 N, applying MVIC reduces the peak and mean values of the force error by 62.56% and 64.03%, respectively. Under working condition ③ and ④, the control effect is most obvious, and the errors elimination ratio of both peak and mean reach nearly 80%, and the control effect does not change obviously with the sinusoidal input force amplitude and frequency change. Under working condition ⑤ to ⑧, the control effect is still obvious, and the periodic variation of the force error is greatly reduced. the errors elimination ratio of both peak and mean reach nearly 50% under all working conditions. Under working condition ⑨ and ⑩, the controller still had a good control effect, the errors elimination ratio of both peak and mean reach nearly 60%, indicating that the MVIC has good robustness.

V. CONCLUSION

In this paper, the MVIC was designed on the basis of the nonlinear mathematical model of the HDU force control system, and the control performance was verified on the HDU performance test platform. Through the above research work, the following conclusions were obtained:

First, the HDU force control system achieved good force tracing performance under different input signals when only adopting a traditional PID controller but had poor robustness under the different disturbance positions. At this point, the force control performance could not satisfy the requirement of high accuracy and high robustness of the servo control of the legged robots.

Second, after adopting the MVIC designed in this paper, the force control performance of the HDU is greatly improved under different sinusoidal working conditions, the average reduction rate of the force control error was generally over 60%, and the control effect did not decrease significantly under different working conditions. Under different random conditions, the force control performance was also greatly improved. The average reduction rate of the force error was generally over 60%, which proved that the MVIC had good adaptability to different working conditions.

Further work: based on the research result in the paper, two aspects of research work will be conducted in the future. First, the control performance of the MVIC designed in the paper when adopting the force-based impedance control method on the robot machine needs further research. Second, the MVIC designed in the paper only aims at the HDU force control system. Whether the same control strategy can be used to improve the position control system remains to be further studied.

REFERENCES

[1] M. Tavakoli *et al.*, "The hybrid OmniClimber robot: Wheel based climbing, arm based plane transition, and switchable magnet adhesion," *Mechatronics*, vol. 36, pp. 136–146, Jun. 2016.
[2] L. Zhang and Y. Qiu, "Design and analysis of small fixed pedrail robot with the variable guide wheel angle," *J. Mech. Transmiss.*, vol. 39, no. 8, pp. 97–110, Aug. 2015.
[3] S. Pan, L. Shi, and S. Guo, "A Kinect-based real-time compressive tracking prototype system for amphibious spherical robots," *Sensors*, vol. 15, no. 4, pp. 8232–8252, Apr. 2015.
[4] K.-X. Ba *et al.*, "Parameters sensitivity analysis of position-based impedance control for bionic legged robots'HDU," *Appl. Sci.*, vol. 7, no. 10, p. 1035, Oct. 2017.
[5] K.-X. Ba, B. Yu, G. Ma, Q. Zhu, Z, Gao, and X, Kong, "A novel position-based impedance control method for bionic legged robots'HDU," *IEEE Access*, vol. 6, pp. 55680–55692, Sep. 2018.
[6] M. Li, Z. Jiang, P. Wang, L. Sun, and S. S. Ge, "Control of a quadruped robot with bionic springy legs in trotting gait," *J. Bionic Eng.*, vol. 11, no. 2, pp. 188–198, Jun. 2014.
[7] H. Kimura, Y. Fukuoka, and A. H. Cohen, "Adaptive dynamic walking of a quadruped robot on natural ground based on biological concepts," *Int. J. Robot. Res.*, vol. 26, no. 5, pp. 475–490, May 2007.
[8] I. Poulakakis, J. A. Smith, and M. Buehler, "Modeling and experiments of untethered quadrupedal running with a bounding gait: The scout II robot," *Int. J. Robot. Res.*, vol. 24, no. 4, pp. 239–256, Apr. 2005.
[9] J. G. Nichol, S. P. N. Singh, K. J. Waldron, L. R. Palmer, III, and D. E. Orin, "System design of a quadrupedal galloping machine," *Int. J. Robot. Res.*, vol. 23, pp. 1013–1027, Jan. 2004.
[10] S. Seok, A. Wang, M. Y. Chuah, D. Otten, J. Lang, and S. Kim, "Design principles for highly efficient quadrupeds and implementation on the MIT cheetah robot," in *Proc. IEEE Int. Conf. Robot. Autom.*, Karlsruhe, Germany, May 2013, pp. 3307–3312.
[11] J. Kim *et al.*, "Development of the lower limbs for a humanoid robot," in *Proc. Int. Conf. Intell. Robots Syst.*, Oct. 2012, pp. 4000–4005.
[12] R. Playter, M. Buehler, and M. Raibert, "BigDog," *Proc. SPIE*, vol. 6230, pp. 62302O-1–62302O-6, May 2006.
[13] C. Semini *et al.*, "Towards versatile legged robots through active impedance control," *Int. J. Robot. Res.*, vol. 34, no. 7, pp. 1003–1020, Jul. 2015.
[14] X. Rong, Y. Li, J. Ruan, and B. Li, "Design and simulation for a hydraulic actuated quadruped robot," *J. Mech. Sci. Technol.*, vol. 26, no. 4, pp. 1171–1177, Apr. 2012.
[15] M. Focchi, V. Barasuol, I. Havoutis, J. Buchli, C. Semini, and D. G. Caldwell, "Local reflex generation for obstacle negotiation in quadrupedal locomotion," in *Proc. Int. Conf. Climbing Walking Robots Support Technol. Mobile Mach.*, 2013, pp. 443–450.
[16] M. Hutter, C. Gehring, M. Bloesch, M. A. Hoepflinger, C. D. Remy, and R. Siegwart, "Starleth: A compliant quadrupedal robot for fast, efficient, and versatile locomotion," in *Proc. 15th Int. Conf. Climbing Walking Robot*, vol. 40, no. 3, Sep. 2012, p. 904.
[17] M. Bajracharya, J. Ma, M. Malchano, A. Perkins, A. A. Rizzi, and L. Matthies, "High fidelity day/night stereo mapping with vegetation and negative obstacle detection for vision-in-the-loop walking," in *Proc. IEEE Int. Conf. Intell. Robots Syst.*, Nov. 2013, pp. 3663–3670.
[18] J. T. Kim, J. S. Cho, B.-Y. Park, S. Park, and Y. Lee, "Experimental investigation on the design of leg for a hydraulic actuated quadruped robot," in *Proc. IEEE Int. Symp. Robot.*, Oct. 2013, pp. 1–5.
[19] G. Wiedebach *et al.*, "Walking on partial footholds including line contacts with the humanoid robot atlas," in *Proc. IEEE-RAS 16th Int. Conf. Humanoids Robots*, Nov. 2016, pp. 1312–1319.
[20] B. Baigzadehnoe, Z. Rahmani, A. Khosravi, and B. Rezaie, "On position/force tracking control problem of cooperative robot manipulators using adaptive fuzzy backstepping approach," *ISA Trans.*, vol. 70, pp. 432–446, Aug. 2017.
[21] J. Li, Y. Wang, X. Wang, J. Shao, T. Yang, and Z. Wang, "Research on electro-hydraulic force servo system based on neural network and fuzzy intelligent control strategy," *J. Comput. Theor. Nanosci.*, vol. 11, no. 4, pp. 1205–1210, Apr. 2014.
[22] D.-P. Li, Y.-J. Liu, S. Tong, C. L. P. Chen, and D.-J. Li, "Neural networks-based adaptive control for nonlinear state constrained systems with input delay," *IEEE Trans. Cybern.*, to be published, doi: 10.1109/TCYB.2018.2799683.
[23] K. K. Ahn and Q. T. Dinh, "Self-tuning of quantitative feedback theory for force control of an electro-hydraulic test machine," *Control Eng. Pract.*, vol. 17, no. 11, pp. 1291–1306, Nov. 2009.
[24] S. Wen, J. Zhu, X. Li, A. B. Rad, and X. Chen "End-point contact force control with quantitative feedback theory for mobile robots," *Int. J. Adv. Robot. Syst.*, vol. 9, no. 1, p. 236, Dec. 2012.
[25] J. Yao, W. Deng, and Z. X. Jiao, "RISE-based adaptive control of hydraulic systems with asymptotic tracking," *IEEE Trans. Autom. Sci. Eng.*, vol. 14, no. 3, pp. 1524–1531, Jul. 2017.
[26] S. Oh and K. Kong, "High-precision robust force control of a series elastic actuator," *IEEE-ASME Trans. Mechatronics*, vol. 22, no. 1, pp. 71–80, Feb. 2017.
[27] K.-X. Ba, B. Yu, Z. Gao, Q. Zhu, G. Ma, and X. Kong, "An improved force-based impedance control method for the HDU of legged robots," *ISA Trans.*, to be published, doi: 10.1016/j.isatra.2018.09.002.
[28] K.-X. Ba *et al.*, "The dynamic compliance and its compensation control research of the highly integrated valve-controlled cylinder position control system," *Int. J. Control Autom. Syst.*, vol. 15, no. 4, pp. 1814–1825, Aug. 2017.
[29] K.-X. Ba *et al.*, "Dynamic compliance analysis for LHDS of legged robot, Part B: Force-based impedance control," *IEEE Access*, vol. 6, pp. 74799–74811, Oct. 2018.

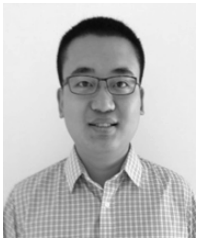

BIN YU received the Ph.D. degree from Yanshan University, China, in 2015. His main research interests include heavy machinery fluid transmission and control and robot design and control.

KAIXIAN BA received the Ph.D. degree from Yanshan University, China, in 2018. His main research interests include electro-hydraulic servo control system and robot design and control.

YALIANG LIU is currently pursuing the master's degree with Yanshan University, China. His main research interests include electro-hydraulic servo control system and robot design and control.

ZHENGGUO JIN is currently pursuing the master's degree with Yanshan University, China. His main research interests include robot design and control.

QIXIN ZHU is currently pursuing the Ph.D. degree with Yanshan University, China. His main research interests include electro-hydraulic servo control system and robot design and control.

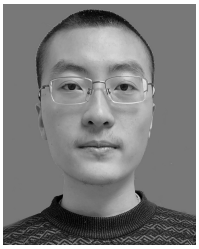

ZHENGJIE GAO is currently pursuing the master's degree with Yanshan University, China. His main research interests include electro-hydraulic servo control system and robot design and control.

GUOLIANG MA is currently pursuing the master's degree with Yanshan University, China. His main research interests include electro-hydraulic servo control system and robot design and control.

XIANGDONG KONG is currently a Professor with Yanshan University, China. His main research interests include electro-hydraulic servo control system, heavy machinery fluid transmission and control, and robot design and control. He serves as the Chairman of the Fluid Transmission and Control Society, which is a branch of the Chinese Mechanical Engineering Society.